



Two-color transparency in a hybrid photothermal cavity system

Ziauddin^{1,a}, Muqaddar Abbas^{1,2,b}, Ayesha Basharat¹, You-Lin Chaung³, Zahida Ehsan⁴, Hamid R. Hamed⁵

¹ Quantum Optics Lab, Department of Physics, COMSATS University Islamabad, Islamabad, Pakistan

² Ministry of Education Key Laboratory for Nonequilibrium Synthesis and Modulation of Condensed Matter, Shaanxi Province Key Laboratory of Quantum Information and Quantum Optoelectronic Devices, School of Physics, Xi'an Jiaotong University, Xi'an 710049, China

³ Physics Division, National Tsing-Hua University, Hsinchu 300, Taiwan

⁴ Landau Feynman Lab for Theoretical Physics, Department of Physics, CUI Lahore Campus, Lahore 54000, Pakistan

⁵ Institute of Theoretical Physics and Astronomy, Vilnius University, Sauletekio 3, 10257 Vilnius, Lithuania

Received: 23 March 2022 / Accepted: 13 July 2022

© The Author(s), under exclusive licence to Società Italiana di Fisica and Springer-Verlag GmbH Germany, part of Springer Nature 2022

Abstract The photothermal effects can make an optical cavity transparent to a weak probe field when a strong driving field is applied (Ma et al. in *Sci. Adv.* 6:eaax8256, 2020). This system provides a photothermal analog of the standard (single) electromagnetically induced transparency. Here, we suggest a novel scenario by introducing into the system a qubit (two-level system), which, besides allowing to achieve the two-color (double) transparency, strongly enhances the transparency effects. When the hybrid system is illuminated by a strong coupling field, the output field is shown to experience both sub- and superluminality at different frequencies.

1 Introduction

Electromagnetically induced transparency (EIT) is a coherent phenomenon in which a stronger control laser induces transparency for a weaker probe laser in an otherwise opaque medium [1–4]. The strong control field creates two dressed states that destructively interfere, leading to a transparency dip for a resonant probe field. EIT has opened a promising avenue to explore various interesting effects, such as slow light propagation [5, 6], photons quantum memory [7], EIT resonance linewidth [8, 9], multiple-EIT [10, 11] and enhancement of optical nonlinearities [12]. Normally, the multiple-EIT appears due to coherent multi-channel in a system that can facilitate long-lived nonlinear interactions.

Similar to the established mechanism for EIT, a controllable transparency effect exists in optomechanical systems with coupled optical and mechanical resonators, known as optomechanically induced transparency (OMIT). The phenomenon of OMIT was first explored in 2010 in a vibrational cavity system [13], and is based on the destructive interference between different paths of the internal fields. The OMIT has been suggested to apply for different purposes, such as quantum router [14], ultraslow light [15], four wave mixing [16], and accurate measurement [17–19]. In addition, two-color (double) OMIT (containing two transparency windows) has been investigated in coupled optomechanical systems [20, 21], and optomechanical systems filled with atomic ensembles [22].

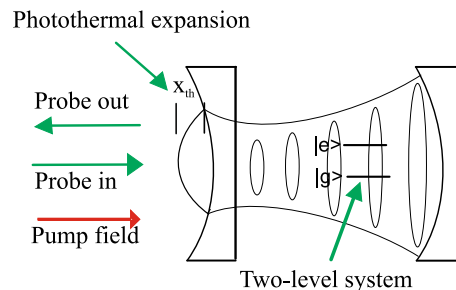
Analogous to EIT and OMIT, the concept of photothermally induced transparency (PTIT) has been recently introduced in a cavity system. This effect occurs when an optical resonator shows a nonlinear behavior because of the optical heating of the mirrors or resonators [23]. Such a transparency, induced by photothermal effects, appears in the presence of a strong optical control field which suppresses the coupling between a weaker optical probe and a resonance feature. Similar to the radiation pressure [24], photothermal effects couple the length of the beam path of the cavity with the intracavity power. This is due to the absorption of photons by the mirrors in the cavity, which leads to thermal expansion and a change in the index of refraction of the coating and the substrate of the mirror. The interference between the pump and probe fields at the frequency difference induces modulation in the cavity optical length, resulting in the anti-Stokes and Stokes fields. Depending on the interaction, the photothermal effect can reduce or increase the cavity optical length [25, 26]. The photothermal-cavity coupling can be used to suppress a microlever's Brownian vibrational fluctuations [27, 28], to achieve the quantum ground state cooling of the mechanical cavity in the bad-cavity limit, and to understand the fundamental limit in gravitational wave detection [31, 32]. Unlike EIT, PTIT does not involve interference between two quantum pathways, and provides possible applications in characterization of photothermal parameters [33] and optical signal processing [34]. The PTIT phenomenon might be also used to extract photo-thermal characteristics, optical amplification, and alteration, and it could even be extended to the quantum regime [23, 27, 28].

In this paper, we theoretically study a rather different situation by injecting into the PTIT setup a qubit. The transmission spectrum of the probe field is very sensitive in the vicinity of a control field frequency, which can be detuned by the cavity frequency. This motivates us to study the possible scheme to modify the cavity frequency. As we know, a qubit is the simplest quantum system, its

^a e-mail: ziauddin@comsats.edu.pk (corresponding author)

^b e-mail: muqaddarabbas@xjtu.edu.cn (corresponding author)

Fig. 1 Schematic representation of the qubit-cavity system. The pump and probe (E_l and E_p) fields are applied from the left to the optical cavity resulting in the photothermal expansion. x_{th} signifies the change in optical cavity length due to expansion of left cavity. Further, $|e\rangle$ and $|g\rangle$ are the excited and ground states of qubit



interaction with a single-mode inside a cavity has been intensely studied based on Jaynes-Cummings model, which is a fundamental theory in cavity quantum electrodynamics. The presence of qubit would change the cavity resonant frequency with the frequency-pulling effect. On the other hand, the corresponding frequency-shift depends on some internal degree of freedom of qubit in such a way that one can control the cavity resonant frequency and the probe transmission in the PTIT. With more degrees of freedom, one can optimize the efficiency of the operation of PTIT. Thus, it provides new possibilities to consider more rich physics behind it. We show that the qubit-cavity interaction can affect the properties of the output probe field, resulting in a two-color (double) transparency and the strongly enhanced transparency effects. The two-color transparency has many applications such as nonlinear wave mixing, cross-phase modulation, optical switching, and wavelength conversion. We study the slow and fast light propagation which can be manipulated via external parameters. The addition of the qubit results in the fast and slow light propagation at two different frequencies when the qubit is initially in the ground state. We also study the slow and fast light propagation when the qubit is initially in the excited state. It is found that such a situation leads to the control of slow and fast light propagation at two different frequencies. Further, the slow and fast light propagation can be tuned effectively by the addition of a qubit in the photothermal cavity, meaning that our suggested system provides an effective approach in controlling the group velocity of the probe light.

2 Model and equations

As schematically depicted in Fig. 1, we consider a theoretical model of a hybrid setup in which a qubit (two-level system) is coupled to single-mode cavity field through Jaynes-Cummings coupling [36]. The left cavity mirror is oriented in such a way that its high-reflectivity coating faces outward and its anti-reflectivity faces inward. The right mirror is attached with a piezoelectric actuator which is used for scanning the length of the cavity. The substrate of the left cavity mirror is made of fused silica. The left cavity mirror is placed inside the cavity leading to the enhancement of photothermal effects. The photothermal cavity under consideration, with a length of L , has a high Q Fabry–Perot. A pair of the weak probe and strong pump fields are shined from the left to the cavity. The fused silica coated on the left mirror from the inside can lead to the expansion of the mirror when the strong pump field is applied, resulting in a change in the refractive index of the substrate. In a proper rotating frame, the Hamiltonian for the whole hybrid qubit-cavity system can be written as

$$\begin{aligned}
 H = & \hbar\Delta_c a^\dagger a - \hbar g_{cp} a^\dagger a x_{th} - \hbar g_{ap} \sigma_z x_{th} \\
 & + \hbar g_{ac} (a^\dagger \sigma_1 + a \sigma_1^\dagger) + \frac{\hbar}{2} \Delta_a \sigma_z + i \hbar E_l (a^\dagger - a) \\
 & + i \hbar E_p (a^\dagger e^{-i\delta t} - a e^{i\delta t}).
 \end{aligned} \tag{1}$$

Here, $\Delta_{c(a)} = \omega_{c(a)} - \omega_l$ correspond to the detuning of the cavity field (atom transition) frequency while $\delta = \omega_p - \omega_l$ represents the detuning of probe field with pump field frequency. In Eq. (1), the first term shows the cavity modes with creation (annihilation) operator $a^\dagger(a)$. The second term indicates the interaction of cavity with the photothermal radiation with the coupling strength g_{cp} . The third term defines the interaction between photothermal expansion with the qubit with $\delta = \omega_p - \omega_l$ the coupling strength g_{ap} . The fourth term shows the interplay of the two-level system with cavity modes with the coupling strength g_{ac} . The fifth term stands for the unperturbed part with the Pauli operator σ_z describing the two-level system with the transition frequency ω_a . The last two terms show the pump and probe fields, with frequencies ω_p and ω_l , respectively, deriving from the left side of the cavity. The probe and pump fields have amplitudes $E_p = \sqrt{2\kappa_1 P_p / \hbar \omega_p}$ and $E_l = \sqrt{2\kappa_1 P_l / \hbar \omega_l}$, respectively. The mirror is heated by the intra-cavity optical field, which causes photothermal displacement. The length of the cavity changes as a result of this displacement, modifying the cavity frequency.

Introducing the cavity and mirror dissipation terms, the equations of the motion read

$$\dot{x}_{th} = -\frac{\gamma_{th}}{m} (x_{th} + \beta \hbar g_{cp} |a|^2 + \beta \hbar g_{ap} \sigma_z), \tag{2a}$$

$$\begin{aligned}
 \dot{a} = & -(\kappa + i\Delta_c) a + i g_{cp} a x_{th} - i g_{ac} \sigma_1 \\
 & + E_l + E_p e^{-i\delta t} + \sqrt{2\kappa} a_{in},
 \end{aligned} \tag{2b}$$

$$\dot{\sigma}_1 = -(\gamma_a + i(\Delta_a - 2g_{ap}x_{th}))\sigma_1 + ig_{ac}a\sigma_z, \tag{2c}$$

where γ_{th} describes the effective photothermal relaxation rates, m is the mass of the mirror, P_c is the intra-cavity power, and $\beta = \partial x_{th} / \partial P_c$ represents the effective photothermal coefficient. In addition, κ represents the cavity decay rates for cavity mode a . The quantum noise operator with zero mean values [30] is described by a_{in} .

To find the steady-state solutions, we consider $x_{th} = x_{ths} + \delta x_{th}$ while the pump field is assumed to be much stronger than the probe field. Here, x_{ths} illustrates the steady-state value governed by the pump field, whereas δx_{th} gives the mean value of fluctuation proportional to the probe field. The same treatment applies to other variables a and σ_1 . The steady-state value of any operator can be attained from Eq. (2) by setting the time derivative to zero, yielding

$$x_{ths} = -\hbar\beta(g_{cp}|a_s|^2 + g_{ap}\langle\sigma_z\rangle_s), \tag{3a}$$

$$a_s = \frac{E_l}{i(\Delta_c - g_{cp}x_{ths} + \kappa) + \frac{g_{ac}^2}{i(\Delta_a - 2g_{ap}x_{ths}) + \gamma_a}}, \tag{3b}$$

$$\sigma_{1s} = \frac{ig_{ac}a_s\langle\sigma_z\rangle_s}{i(\Delta_a - 2g_{ap}x_{ths}) + \gamma_a}, \tag{3c}$$

where $\sigma_z = |e\rangle\langle e| - |g\rangle\langle g|$. Let us first consider the case when the quantum two-level system is initially in its ground state i.e., $\sigma_z = -1$. The linearized equations read

$$\delta\dot{x}_{th} = -\frac{\gamma_{th}}{m}(\delta x_{th} + \hbar\beta g_{cp}(a_s\delta a^* + a_s^*\delta a) - \hbar\beta g_{ap}), \tag{4a}$$

$$\begin{aligned} \delta\dot{a} = & -(\kappa\delta a + i(\Delta_c\delta a - g_{cp}(x_{ths}\delta a + \delta x_{th}a_s))) \\ & - ig_{ac}\delta\sigma_1 + E_l + E_p e^{-i\delta t}, \end{aligned} \tag{4b}$$

$$\delta\dot{\sigma}_1 = -(\gamma_a\delta\sigma_1 + i(\Delta_a\delta\sigma_1 - 2g_{ap}(x_{ths}\delta\sigma_1 + \delta x_{th}\sigma_{1s}))), \tag{4c}$$

To solve the above linear equations, we use the ansatz

$$\begin{aligned} \delta a &= \delta a_- e^{-i\delta t} + \delta a_+ e^{i\delta t}, \\ \delta x_{th} &= \delta x_- e^{-i\delta t} + \delta x_+ e^{i\delta t}, \\ \delta\sigma &= \delta\sigma_- e^{-i\delta t} + \delta\sigma_+ e^{i\delta t}. \end{aligned} \tag{5}$$

Using the ansatz in Eq. (5) one gets

$$(\kappa + i(\Delta_c - g_{cp}x_{ths}) - i\delta)\delta a_- - ig_{cp}a_s x_- + ig_{ac}\sigma_{1-} - E_p = 0, \tag{6a}$$

$$\left(\frac{\gamma_{th}}{m} - i\delta\right)x_- + \left(\frac{\gamma_{th}}{m}\right)(\hbar\beta g_{cp})(a_s\delta a_+^* + a_s^*\delta a_-) = 0, \tag{6b}$$

$$(\gamma_a + i(\Delta_a - 2g_{ap}x_{ths}) - i\delta)\sigma_{1-} - 2ig_{ap}\sigma_{1s}x_- + ig_{ac}\delta a_- = 0, \tag{6c}$$

$$(\kappa - i(\Delta_c - g_{cp}x_{ths}) - i\delta)\delta a_+^* + ig_{cp}a_s^* x_+^* - ig_{ac}\sigma_{1+}^* = 0, \tag{6d}$$

$$\left(\frac{\gamma_{th}}{m} - i\delta\right)x_+^* + \left(\frac{\gamma_{th}}{m}\right)(\hbar\beta g_{cp})(a_s^*\delta a_- + a_s\delta a_+^*) = 0, \tag{6e}$$

$$(\gamma_a - i(\Delta_a - 2g_{ap}x_{ths}) - i\delta)\sigma_{1+}^* + 2ig_{ap}\sigma_{1s}^*x_+^* - ig_{ac}\delta a_+^* = 0. \tag{6f}$$

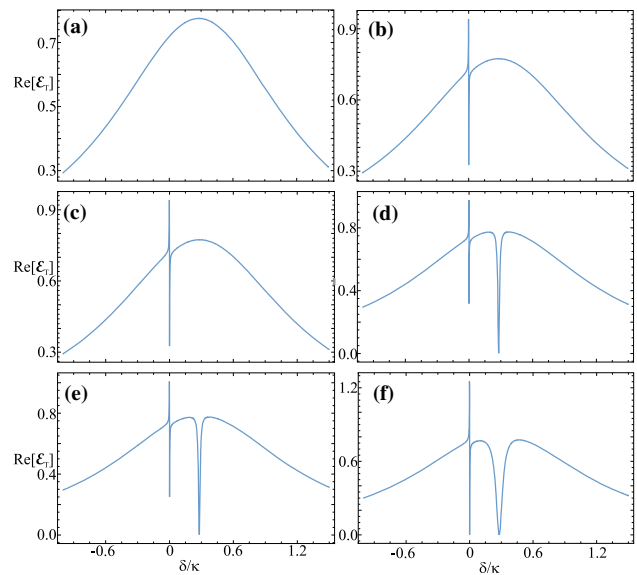
Solving the above coupled equations, we can find the expression for δa_- as

$$\begin{aligned} \delta a_- = & [E_p\alpha_4(g_{ac}^2\alpha_2 + \alpha_2\alpha_5\alpha_6a_s^* + 2a_sg_{ac}g_{ap}\alpha_3\sigma_{1s}^*)]/[(g_{ac}^4 \\ & \times \alpha_2 + g_{ac}^2\alpha_1\alpha_2\alpha_4 + g_{ac}^2\alpha_2\alpha_5\alpha_6 + \alpha_1\alpha_2\alpha_4\alpha_5\alpha_6 + 2g_{ac}^3g_{ap}\sigma_{1s} \\ & \times \alpha_3\alpha_5\alpha_6a_s^* + ia_sg_{cp}\alpha_3\alpha_4\alpha_5\alpha_6a_s^* + 2a_sg_{ac}g_{ap}\alpha_1\alpha_3\alpha_4\sigma_s^*)], \end{aligned} \tag{7}$$

with

$$\begin{aligned} \alpha_1 &= \kappa + i\Delta_{01} - i\delta, \\ \alpha_2 &= \frac{\gamma_{th}}{m} - i\delta, \\ \alpha_3 &= \frac{\gamma_{th}}{m}(\beta g_{cp}), \\ \alpha_4 &= \gamma_a + i\Delta_{02} - i\delta, \\ \alpha_5 &= \kappa - i\Delta_{01} - i\delta, \\ \alpha_6 &= \gamma_a - i\Delta_{02} - i\delta, \end{aligned} \tag{8}$$

Fig. 2 The $\text{Re}[\mathcal{E}_T]$ versus δ/κ when all the coupling parameters are set to **a** zero, **b** $g_{cp}/2\pi = 2$ MHz and $g_{ap} = g_{ac} = 0$, **c** $g_{cp}/2\pi = 2$ MHz, $g_{ap}/2\pi = 1.5$ MHz and $g_{ac}/2\pi = 0$, **d** $g_{cp}/2\pi = 2$ MHz, $g_{ap}/2\pi = 0$ and $g_{ac}/2\pi = 0.05$ MHz, **e** $g_{cp}/2\pi = 2$ MHz, $g_{ap}/2\pi = 1.5$ MHz and $g_{ac}/2\pi = 0.05$ MHz, **f** $g_{cp}/2\pi = 2$ MHz, $g_{ap}/2\pi = 1.5$ MHz and $g_{ac}/2\pi = 0.1$ MHz. The other parameters are $\Delta_{01} = 0.28\kappa$, $\Delta_{02} = 0.28\kappa$, $\kappa/2\pi = 530$ kHz, $\beta = -1.8$ pm/W, $\gamma_{th}/2\pi = 15.9$ Hz, $E_l/2\pi = 0.5$ MHz, $\gamma_a/2\pi = 2$ Hz, $\Delta_c/2\pi = 10$ MHz, and $\Delta_a/2\pi = 10$ MHz



where $\Delta_{01} = \Delta_c - g_{cp}x_{ths}$ and $\Delta_{02} = \Delta_a - 2g_{ap}x_{ths}$ are the effective detuning. Similar expressions can be obtained when we assume the two-level system is initially prepared in its excited state $\sigma_z = 1$ (not shown here).

We can write the input-output relation of the cavity as [37]

$$E_{out}(t) + E_p e^{-i\delta t} + E_l = \sqrt{2\kappa}\delta a, \tag{9}$$

where

$$E_{out}(t) = E_{out}^0 + E_{out}^+ E_p e^{-i\delta t} + E_{out}^- E_p e^{i\delta t}. \tag{10}$$

Solving Eqs. (9) and (10), we find

$$E_{out}^+ = \frac{\sqrt{2\kappa}\delta a_-}{E_p} - 1. \tag{11}$$

Further we define

$$E_{out}^+ + 1 = \frac{\sqrt{2\kappa}\delta a_-}{E_p} = \mathcal{E}_T. \tag{12}$$

Here, the quadratures of the field \mathcal{E}_T may be written as $\mathcal{E}_T = u_p + i v_p$, where u_p and v_p are the in-phase and out-of-phase quadratures of the output probe field, respectively, while u_p and v_p represent the absorptive and dispersive characteristics of the probe field when propagating through the cavity.

3 Results and discussion

3.1 The two-level system is initially in the ground state

In this section, we study the characteristics of the output probe field under the influence of different coupling strengths i.e., cavity-photothermal coupling (g_{cp}), atom-photothermal coupling (g_{ap}), and atom-cavity coupling (g_{ac}). In the absence of the strong driving field, all the coupling parameters might be set to zero. Therefore, we consider all the coupling parameters are zero and plot in Fig. 2a the $\text{Re}[\mathcal{E}_T]$ versus probe field detuning δ/κ . We get a Lorentzian profile indicating that the probe field is completely absorbed inside the cavity, that is the typical response of the bare cavity. In the presence of strong control field and by considering $g_{cp} \neq 0$, again we plot the $\text{Re}[\mathcal{E}_T]$ versus probe field detuning δ/κ as shown in Fig. 2b. The profile of the output probe field shows that the Lorentzian response is modified and we get a transparency window. The narrow transparency is obtained when the control and probe field frequencies are very close to each other i.e., $\delta \approx 0$. While this behavior is somehow similar to EIT and OMIT, it is rather different. In the case of OMIT, the beating frequency of control and probe becomes equal to the optomechanical frequency, whereas the transparency occurs in the photothermal cavity when the probe field is very close to the control field [23]. This is due to the fact that the beating of the probe and strong driving fields generates the oscillation of the effective cavity length via photothermal effects. The oscillation induces the Stokes and anti-Stokes fields where the probe and Stokes fields generate the destructive interference and

leads to a transparency window. In the absence of coupling strength g_{ac} , we look for the influence of g_{ap} on the output spectrum as shown in Fig. 2c. The spectrum shows that g_{ap} does not matter if g_{ac} is absent. Next, we switch on the coupling strength g_{ac} while $g_{ap} = 0$ and plot in Fig. 2d the $\text{Re}[\mathcal{E}_T]$ versus δ/κ . In the presence of g_{ac} , a new transparency window takes place in the $\text{Re}[\mathcal{E}_T]$ profile. This transparency window occurs via the interaction of the qubit with the cavity. This is due to the fact that when the probe frequency is resonant with the qubit frequency it can result in a transparency window. The two-color transparency also appear when both coupling strength g_{cp} and g_{ac} are present (see Fig. 2e, f). Enhanced transparency effects are observed by increasing the width and depth of transparency windows through proper manipulating both g_{cp} and g_{ac} values.

3.2 Slow and fast light

We have already discussed the characteristics of the output probe field when the probe field is propagating through the cavity. As it is shown, the double transparency windows are achieved under the effect of the coupling strengths g_{cp} and g_{ac} . The presence of two transparency windows implies that there might be a modification of the cavity dispersion. It is already established that the positive slope of dispersion corresponds to the slow light propagation while the negative slope of dispersion determines the advance or fast light propagation. The group delay (or advance) corresponding to the probe field can be defined as [13]

$$\tau_g = \frac{d\varphi_t(\omega_p)}{d\omega_p}, \quad (13)$$

where $\varphi_t(\omega_p) = \arg[t(\omega_p)]$ is the phase of the output probe field and

$$t(\omega_p) = 1 - \frac{\sqrt{2\kappa}\delta a_-}{E_p}. \quad (14)$$

In expression (13), the magnitude of the group delay is dependent on the rapid phase change in the output probe field. This indicates that the sign of τ_g determines the characteristics of the probe light. In other words, a negative value of the group delay is corresponding to the advancement of the probe field while a positive value of the group delay is corresponding to the slow light propagation. In the following, we study the phase and group delay or advance of probe light using Eq. (13) for different system parameters. When all the coupling parameters are set to zero, we get a negative slope of dispersion with a negative group delay in the spectrum, as can be seen in Fig. 3a, b. This is the case in which a Lorentzian profile appears in the transmission spectrum (see Fig. 2a). Transparency occurs when the coupling strength is nonzero ($g_{cp} \neq 0$). In this case, a steep negative dispersion appears around $\delta/\kappa \approx 0$, see Fig. 3c. A maximum group advance of about 3000 μs is also achieved (Fig. 3d). Next, we consider that all the coupling parameters are nonzero and plot in Fig. 3e, f the phase and group delay profiles against δ/κ . We observe both negative and positive slopes at different frequencies. The negative slope occurs due to the coupling strength g_{cp} , whereas the positive slope is because of the coupling strength g_{ac} . Similarly, we achieved a group advance for the negative slope while a group delay for the positive slope at different frequencies. The phase and group delay may be affected via the manipulation of coupling strength g_{cp} . Changing in Fig. 3g, h the coupling strength $g_{cp}/2\pi$ from 1 to 3 MHz (with all other parameters unchanged), we can see an increase in the group delay while a decrease in the group advance.

3.3 The two-level system is initially in the excited state

Thus far we have considered the two-level system is initially in the ground state. In what follows, we consider a different situation in which the qubit is prepared in the excited state i.e., $\sigma_z = 1$. The profiles for the transparency (absorption) are approximately similar to the previous case illustrated in Fig. 2, yet the phase and group delay characteristics behave differently. In Fig. 4a, b, we show the spectrum of phase and τ_g of the probe field versus δ/κ by considering $g_{cp}/2\pi = 1$ MHz, $g_{ap}/2\pi = 1.5$ MHz and $g_{ac}/2\pi = 0.01$ MHz. By considering $\sigma_z = 1$, we obtain negative slope of dispersion at different frequencies, see Fig. 4a. At frequency $\delta/\kappa \approx 0.28$ MHz, we get negative slope of dispersion, whereas for previous case (when $\sigma_z = -1$) positive of slope dispersion was achieved. Obviously, when the system is initially in the excited state, a negative slope is also achieved with a group advance at $\delta/\kappa \approx 0.28$ MHz as shown in Fig. 4b. By increasing the coupling strength g_{cp} from $g_{cp}/2\pi = 1$ MHz to $g_{cp}/2\pi = 5$ MHz we find that the phase and group advance modify only around $\delta/\kappa \approx 0$ as this phase and group delay occurs via the coupling strength g_{cp} .

4 Possible applications

As reported earlier, the photothermal effect is effective in quenching the Brownian fluctuation of mechanical oscillators [38, 39]. Moreover, one can characterize the photothermal parameters such as photothermal relaxation rate and photothermal coefficient by the frequency modulation of input laser or by the expansion of photothermal effect that leads to change in the cavity length. The phenomenon of PTIT [23] is easy to access experimentally and paves the way toward applications in classical signal processing such as filtering and optical amplification. Introducing a qubit in the photothermal cavity can strengthen the coupling, leading to enhancing the nonlinearity. Therefore, the interaction of qubit to the photothermal cavity may provide further applications in classical

Fig. 3 **a** The phase and **b** group delay versus δ/κ when all the coupling parameters are equal to zero; **c** the phase and **d** group delay versus δ/κ when $g_{cp}/2\pi = 1$ MHz, $g_{ap}/2\pi = 1.5$ MHz, and $g_{ac}/2\pi = 0$; **e** the phase and **f** group delay versus δ/κ when $g_{cp}/2\pi = 1$ MHz, $g_{ap}/2\pi = 1.5$ MHz, and $g_{ac}/2\pi = 0.01$; **g** the phase and **h** group delay versus δ/κ when $g_{cp}/2\pi = 3$ MHz, $g_{ap}/2\pi = 1.5$ MHz, and $g_{ac}/2\pi = 0.01$. The other parameters are the same as in Fig. 2

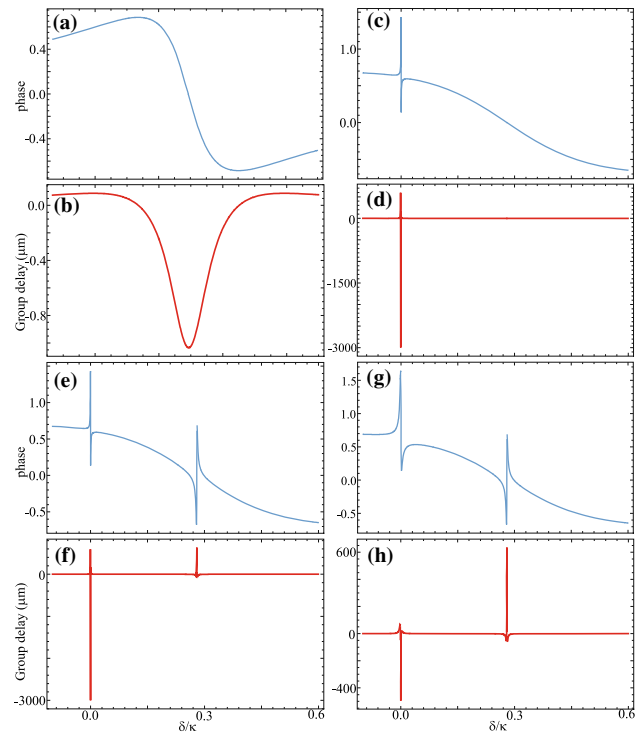
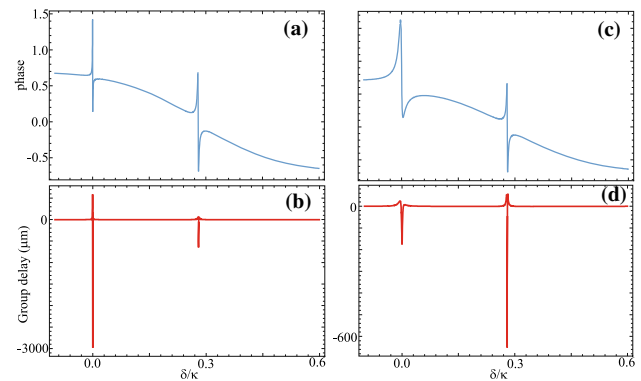


Fig. 4 **a** The phase and **b** group delay versus δ/κ when $g_{cp}/2\pi = 1$ MHz, $g_{ap}/2\pi = 1.5$ MHz, and $g_{ac}/2\pi = 0.01$ MHz; **c** the phase and **d** group delay versus δ/κ when $g_{cp}/2\pi = 5$ MHz, $g_{ap}/2\pi = 1.5$ MHz, and $g_{ac}/2\pi = 0.01$ MHz. The remaining parameters are the same as in Fig. 2



processing. Also, our results show the modification and controlling of slow and fast light propagation, and can be easily achieved experimentally [23, 29]. Motivated by the experiments [23, 29], our scheme might be realizable experimentally. The other unique feature of this scheme is that it is compact and versatile, enabling a quick and precise characterization of photothermal effects. Additionally, photothermal effects have been reported to involve many other phenomena, such as self-sustained oscillations, chaos, production of squeezed light, etc. All these effects contribute to the birth of photothermal optics. The transmission spectrum of the probe field is very sensitive to the control field frequency, which can be detuned by cavity resonant frequency. The presence of any quantum objects would change the transmission spectrum such that it is possible to apply this system to be a single molecule sensor for which electronic transition of the unknown chemical molecules can be detected from the transmission spectrum precisely.

5 Conclusion

We have studied theoretically the characteristics of the output probe field by considering a two-level system inside a photothermal cavity. It has been shown that the probe field characteristics can be manipulated by adjusting different parameters such as g_{cp} , g_{ap} and g_{ac} . By tuning the coupling parameters, we get double transparency windows simultaneously at different frequencies. Further, by tuning the coupling parameters we control the slow and fast light simultaneously at different frequencies. Our model paves the way toward further theoretical and experimental studies to explore the PTIT as well as new stimulating phenomena in photothermal cavity systems.

References

1. S.E. Harris, J.E. Field, A. Imamoglu, *Phys. Rev. Lett.* **64**, 1107 (1990)
2. K.-J. Boller, A. Imamoglu, S.E. Harris, *Phys. Rev. Lett.* **66**, 2593 (1991)
3. S.E. Harris, *Phys. Today* **50**(7), 36 (1997)
4. M. Fleischhauer, A. Imamoglu, J.P. Marangos, *Rev. Mod. Phys.* **77**, 633 (2005)
5. O. Kocharovskaya, Y. Rostovtsev, M.O. Scully, *Phys. Rev. Lett.* **86**, 628 (2001)
6. A.V. Turukhin, V.S. Sudarshanam, M.S. Shahriar, J.A. Musser, B.S. Ham, P.R. Hemmer, *Phys. Rev. Lett.* **88**, 023602 (2001)
7. A.I. Lvovsky, B.C. Sanders, W. Tittel, *Nat. Photonics* **3**, 706 (2009)
8. J. Anupriya, N. Ram, M. Pattabiraman, *Phys. Rev. A* **81**, 043804 (2010)
9. T.G. Akin, S.P. Krzyzewski, A.M. Marino, E.R.I. Abraham, *Opt. Commun.* **339**, 209 (2015)
10. Y. Chang, C.P. Sun, *Phys. Rev. A* **83**, 053834 (2011)
11. S. Hughes, G.S. Agarwal, *Opt. Lett.* **43**, 5953 (2018)
12. M. Jain, H. Xia, G.Y. Yin, A.J. Merriam, S.E. Harris, *Phys. Rev. Lett.* **77**, 4326 (1996)
13. S. Weis, R. Riviere, S. Deleglise, E. Gavartin, O. Arcizet, A. Schliesser, T.J. Kippenberg, *Science* **330**, 1520 (2010)
14. G.S. Agarwal, S. Huang, *Phys. Rev. A* **85**, 021801(R) (2012)
15. J.D. Teufel, D. Li, M.S. Allman, K. Cicak, A.J. Sirois, J.D. Whittaker, R.W. Simmonds, *Nature (London)* **471**, 204 (2011)
16. S.M. Huang, G.S. Agarwal, *Phys. Rev. A* **81**, 033830 (2010)
17. J.Q. Zhang, Y. Li, M. Feng, Y. Xu, *Phys. Rev. A* **86**, 053806 (2012)
18. Q. Wang, W.J. Li, P.C. Ma, Z. He, *Int. J. Theor. Phys.* **56**, 2212 (2017)
19. J.X. Peng, Z. Chen, Q.Z. Yuan, X.L. Feng, *Phys. Rev. A* **99**, 043817 (2019)
20. S. Shahidani, M.H. Naderi, M. Soltanolkotabi, *Phys. Rev. A* **88**, 053813 (2013)
21. K. Ullah, H. Jing, F. Saif, *Phys. Rev. A* **97**, 033812 (2018)
22. H. Wang, X. Gu, Y.X. Liu, A. Miranowicz, F. Nori, *Phys. Rev. A* **90**, 023817 (2014)
23. J. Ma, J. Qin, G.T. Campbell, R. Lecamwasam, K. Sripathy, J. Hope, B.C. Buchler, P.K. Lam, *Sci. Adv.* **6**, eaax8256 (2020)
24. G. Guccione, M. Hosseini, S. Adlong, M.T. Johnsson, J. Hope, B.C. Buchler, P.K. Lam, *Phys. Rev. Lett.* **111**, 183001 (2013)
25. K. Konthasinghe, J.G. Velez, A.J. Hopkins, M. Peiris, L.T.M. Profeta, Y. Nieves, A. Muller, *Phys. Rev. A* **95**, 013826 (2017)
26. K. An, B. Sones, C. Fang-Yen, R. Dasari, M. Feld, *Opt. Lett.* **22**, 1433 (1997)
27. C.H. Metzger, K. Karrai, *Nature* **432**, 1002 (2004)
28. M. Pinard, A. Dantan, *New J. Phys.* **10**, 095012 (2008)
29. J.-M. Pirkkalainen, S.U. Cho, F. Massel, J. Tuorila, T.T. Heikkila, P.J. Hakonen, M.A. Sillanpää, *Nat. Commun.* **6**, 6981 (2015)
30. M. Aspelmeyer, T.J. Kippenberg, F. Marquardt, *Rev. Mod. Phys.* **86**, 1391 (2014)
31. M. Cerdonio, L. Conti, A. Heidmann, M. Pinard, *Phys. Rev. D* **63**, 082003 (2001)
32. M. De Rosa, L. Conti, M. Cerdonio, M. Pinard, F. Marin, *Phys. Rev. Lett.* **89**, 237402 (2002)
33. H. Schuessler, S. Chen, Z. Tang, E. Benck, *App. Opt.* **31**, 2669 (1992)
34. V. Van, T. Ibrahim, P. Absil, F. Johnson, R. Grover, P.T. Ho, *IEEE J. Sel. Top. Quantum Electron.* **8**, 705 (2002)
35. K. Qu, G.S. Agarwal, *Phys. Rev. A* **87**, 031802 (2013)
36. S. Haroche, J.M. Raimond, *Exploring the Quantum: Atoms, Cavities, and Photons* (Oxford University, Oxford, 2006), M.O. Scully, M.S. Zubairy, *Quantum Optics*, Cambridge University Press, Cambridge, UK, (1997)
37. D. F. Walls, G. J. Milburn, *Quantum Optics* (Springer, 2008)
38. C.H. Metzger, K. Karrai, *Nature* **432**, 1002 (2004)
39. M. Hosseini, G. Guccione, H.J. Slatyer, B.C. Buchler, P.K. Lam, *Nat. Commun.* **5**, 4663 (2014)

Springer Nature or its licensor holds exclusive rights to this article under a publishing agreement with the author(s) or other rightsholder(s); author self-archiving of the accepted manuscript version of this article is solely governed by the terms of such publishing agreement and applicable law.